Biomaterials 29 (2008) 4584–4591

Contents lists available at ScienceDirect

Biomaterials

journal homepage: www.elsevier.com/locate/biomaterials

Viscoelastic adhesive mechanics of aldehyde-mediated soft tissue sealants

Tarek M. Shazly [a,*], Natalie Artzi [a], Fiete Boehning [a], Elazer R. Edelman [a,b]

[a] Biomedical Engineering Center, Harvard-MIT Division of Health Sciences and Technology, Massachusetts Institute of Technology, Cambridge, MA 02139, United States
[b] Cardiovascular Division, Department of Medicine, Brigham and Women's Hospital, Harvard Medical School, Boston, MA 02115, United States

ARTICLE INFO

Article history:
Received 18 July 2008
Accepted 22 August 2008
Available online 19 September 2008

Keywords:
Adhesion
Adhesion mechanics
Hydrogel
Viscoelasticity

ABSTRACT

Soft tissue sealants generally sacrifice adhesive strength for biocompatibility, motivating the development of materials which interact with tissue to a predictable and controllable extent. Crosslinked hydrogels comprising aminated star polyethylene glycol and high molecular weight dextran aldehyde polymers (PEG:dextran) display aldehyde-mediated adhesion and readily tunable reactivity with soft tissue ex-vivo. Evaluation of PEG:dextran compositional variants revealed that the burst pressure of repaired intestinal wounds and the extent of material-induced tissue deformation both increase non-linearly with formulation aldehyde content and are consistently within the desired range established by traditional sealants. Adhesive test elements featuring PEG:dextran and intestinal tissue exhibited considerable viscoelasticity, prompting use of a standard linear solid (SLS) model to describe adhesive mechanics. Model elements were accurately represented as continuous functions of PEG:dextran chemistry, facilitating prediction of adhesive mechanics across the examined range of compositional formulations. SLS models of traditional sealants were also constructed to allow general correlative analyses between viscoelastic adhesive mechanics and metrics of sealant performance. Linear correlation of equilibrium SLS stiffness to sealant-induced tissue deformation indicates that dense adhesive crosslinking restricts tissue expansion, while correlation of instantaneous SLS stiffness to burst pressure suggests that the adhesive stress relaxation capacity of PEG:dextran enhances their overall performance relative to traditional sealants.

1. Introduction

Adhesive sealants assist tissue repair and reduce operative risk through anastomotic stabilization, promotion of wound healing between disjoined tissues, and induction of rapid hemostasis [1–3]. Bioadhesive properties are largely a consequence of material reactivity with tissue, and as a result controlling unintended and deleterious reactivity is a major challenge of sealant design [4]. Tradeoffs between various adhesive properties dependent on bioreactivity are exemplified by common cyanoacrylate- and fibrin-based sealants [5–7]. Cyanoacrylate derivatives are highly bioreactive and adhere strongly to tissue, but are clinically limited due to excessive inflammation upon application and the release of cytotoxic by-products [8,9]. Fibrin sealants are generally more biocompatible, but weakly adhere to tissue and introduce a risk of infectious transmission given their biological origin [2,10–12]. A clear need persists for a soft tissue sealant capable of high strength and prolonged adhesion with minimal immune or inflammatory response.

Limitations of existing sealants could in part reflect a disturbance in underlying tissue mechanics following adhesive bond formation. Many soft tissues are viscoelastic and entropically dissipate significant amounts of mechanical stress under physiologic loading [13–16]. Highly reactive cyanoacrylate derivatives achieve relatively high strength bioadhesion but in doing so may reduce native viscoelasticity as a consequence of low molecular weight tissue crosslinking. Conversely, less adherent fibrin sealants will likely maintain tissue viscoelasticity but cannot provide the mechanical strength necessary for wound stabilization and other clinical applications [17]. A viscoelastic model of adhesive mechanics could meaningfully describe tissue–material interactions and facilitate correlation of mechanical properties with ultimate function.

Biomaterial applications of both star polyethylene glycol (PEG) and various polysaccharides have been extensively studied [18–23]. Clinical interest in these materials has emerged because of their excellent biocompatibility, readily modifiable chemistries, and capability to form tissue-like hydrogel matrices. Here, crosslinked hydrogels composed of various ratios of aminated star PEG and dextran aldehyde polymers (PEG:dextran) were evaluated as potential soft tissue sealants with tunable adhesive properties [24,25]. We hypothesized that the aldehyde content of PEG:dextran

* Corresponding author. Tel.: +1 617 258 8895; fax: +1 617 253 2514.
E-mail address: shazly@mit.edu (T.M. Shazly).

0142-9612/$ – see front matter © 2008 Elsevier Ltd. All rights reserved.
doi:10.1016/j.biomaterials.2008.08.032

hydrogels will heavily influence their adhesion, and that the large reactive polymer constituent (10 kDa dextran aldehyde) will allow viscoelastic adhesive crosslinking. Adhesion of PEG:dextran to soft tissue should contrast the effect of small aldehyde-based fixatives, such as formaldehyde and glutaraldehyde, which tightly crosslink tissues and radically alter their physical and mechanical properties [26].

A series of PEG:dextran formulations with increasing aldehyde content were synthesized to examine the impact of aldehyde-mediated interactions on adhesive properties. Burst pressure of repaired intestinal wounds and the extent of material-induced tissue deformation served as ex-vivo metrics of sealant performance. Tensile testing of adhesive constructs was used to probe the viscoelastic properties of PEG:dextran–tissue interactions and allow development of a standard linear solid (SLS) model relating adhesive mechanics to material chemistry. Additional mechanical testing and SLS modeling of traditional fibrin and octyl-cyanoacrylate sealants promoted general relation of viscoelastic adhesive mechanics to ex-vivo performance metrics. Correlative analyses revealed that adhesive bond density is a primary determinant of sealant functionality, and further suggested that overall performance is enhanced through operational stress relaxation mechanisms following PEG:dextran adhesion to soft tissue.

2. Materials and methods

2.1. Synthesis and network formation of PEG:dextran

The synthesis of star PEG amine and dextran aldehyde as well as the network formation of PEG:dextran has been previously described [24,25]. Briefly, eight-arm, 10 kDa star PEG polymer with amine end groups was dissolved in water to form a 25 wt% aqueous solution. Linear dextran (10 kDa) was oxidized with sodium periodate to yield dextran aldehyde polymer (50% oxidation of glucose rings, 2 aldehyde groups per oxidized glucose ring), which was also prepared as an aqueous solution (2.95–20.65 wt%). The two homogeneous polymer solutions were loaded into a dual-chamber syringe equipped with a 12-step mixing tip. PEG:dextran network formation occurs within seconds to minutes following the injection and controlled mixing of PEG amine and dextran aldehyde via a Schiff's base reaction between the constituent reactive groups (aldehydes and amines).

2.2. Selection and designation of PEG:dextran variants

Compositional variables of both star PEG amine and dextran aldehyde are easily manipulated in the synthesis of PEG:dextran. The solid contents, molecular weights, and reactive group content of polymer constituents are readily altered to achieve crosslinked networks with distinct material properties [24,25]. The present study focused on examining the effects of relative aldehyde concentration on adhesive mechanics, motivating the synthesis of a series of material formulations with isolated variation in dextran aldehyde solid content. As star PEG amine compositional variables (and consequently amine group concentrations) are held constant, the formulations under study are meaningfully differentiated by the ratio of aldehyde to amine reactive group concentrations, designated as $CHO:NH_2$ (Table 1).

2.3. Wounding, repair, and dynamic loading of intestinal tissue

Adult Sprague-Dawley rats (250–300 g, Charles River Laboratories, MA) were sacrificed via carbon dioxide asphyxiation under university IACUC protocol and federal guidelines for animal care. Following sacrifice, the duodenum was immediately excised and immersed in 10 ml Krebs–Henseleit buffer at room temperature. Longitudinal duodenal segments were cut and inserted into a mechanical testing apparatus configured for luminal perfusion (Bose® Biodynamic Test Instrument, Minnetonka, MN). A wound was introduced by full-thickness puncturing of the intestinal wall with an 18 gauge needle. Wounds were then repaired with a 200 μl application of PEG:dextran, octyl-cyanoacrylate (Dermabond, Ethicon Inc.), or fibrin sealant (Calbiochem) to the outer intestinal surface. A 5 min sealant curing time was allowed, after which pulsatile loads were applied through controlled perfusion of the intestine lumen with phosphate buffered saline (PBS). All repair sites featuring PEG:dextran variants remained intact throughout loading, substantiating clinical potential of these materials as a soft tissue sealing agent (Fig. 1A).

2.4. Measurement of burst pressure and tissue deformation

The burst pressure of repaired intestinal wounds (prepared and treated as above) was measured through gradual increase of lumen pressure. A slow development of pressure was achieved through restriction of flow distal to the sample lumen and monitored at the inlet of the intestine. The burst pressure was easily detected in this manner, as failure of the repair site resulted in an immediate loss of developed inlet pressure and visible PBS leakage. The maximum luminal pressure prior to interface failure was recorded as the wound burst pressure.

The tissue response to wound repair and loading was assessed through histological processing (hematoxylin and eosin stain) and numerical image analyses (Matlab, Mathworks Inc.) of intestinal samples. The reduction of lumen area directly adjacent to the material application site was chosen as a performance metric to indicate the extent to which wound repair and loading altered local tissue architecture.

2.5. Stress relaxation of intestinal tissue and bulk PEG:dextran

Intestinal ring samples were prepared by transversely sectioning rat duodenum immediately after sacrifice and tissue excision. Ring samples of approximately 3 mm width were inserted into a mechanical testing apparatus configured for tensile testing (Bose® Biodynamic Test Instrument, Minnetonka, MN). Tissue samples were fixed in the mechanical tester such that the displacement axis was coincident with the ring radial direction. A programmed step displacement was used to impart a 0.2 tensile strain for 6 min, with continuous acquisition (scan rate of 50/s) of the resultant force via the system load cell and software package (WinTest® Software, Minnetonka, MN). Mechanical data were processed to yield a tissue stress relaxation curve.

The viscoelastic response of a representative PEG:dextran material was also analyzed under constant applied displacement. Test samples were prepared by polymerization of PEG:dextran in Lexan strip molds with oversized ends, allowing secure attachment to soft-sample clamps of the mechanical testing apparatus. Following a cure time of 5 min, strip samples were moderately hydrated with a 10 ml PBS rinse over surfaces within the test region. As before, a tensile strain of 0.2 was applied for 6 min through a programmed step displacement. The resultant load data were acquired and processed to yield a bulk PEG:dextran stress relaxation curve.

2.6. Bulk PEG:dextran stiffness

Ramped uniaxial displacements (displacement rate of 0.05 mm/s) were applied to bulk strip samples of PEG:dextran materials (prepared and treated as above) with a mechanical testing apparatus configured for tensile testing (Bose® Biodynamic Test Instrument, Minnetonka, MN). Resultant force and displacement data were continuously recorded (scan rate 200/s) throughout mechanical testing by the system load cell and software package (WinTest® Software, Minnetonka, MN). Force versus displacement data were transformed into true stress versus strain for each test sample, facilitating calculation of bulk elastic moduli.

2.7. PEG:dextran gelation time

The gelation times of PEG:dextran formulations were determined through constant agitation and visual monitoring of material components undergoing network formation. Material samples were injected into glass plates through dual-chamber syringes equipped with mixing tips. A magnetic stir rod was used to agitate

Table 1
Compositional description of the examined five-material series of PEG:dextran

PEG amine				Dextran aldehyde				PEG:dextran
Arm Number (#)	Molecular Weight (kDa)	Solid Content (%)	Amine Content (# per ml)	Molecular Weight (kDa)	Percent Oxidation (%)	Solid Content (%)	Aldehyde Content (# per ml)	Reactive Group Ratio ($CHO:NH_2$)
8	10	25	1.2×10^{20}	10	50	2.95	1.2×10^{20}	1
8	10	25	1.2×10^{20}	10	50	5.90	2.4×10^{20}	2
8	10	25	1.2×10^{20}	10	50	8.85	3.6×10^{20}	3
8	10	25	1.2×10^{20}	10	50	14.75	6.0×10^{20}	5
8	10	25	1.2×10^{20}	10	50	20.65	8.4×10^{20}	7

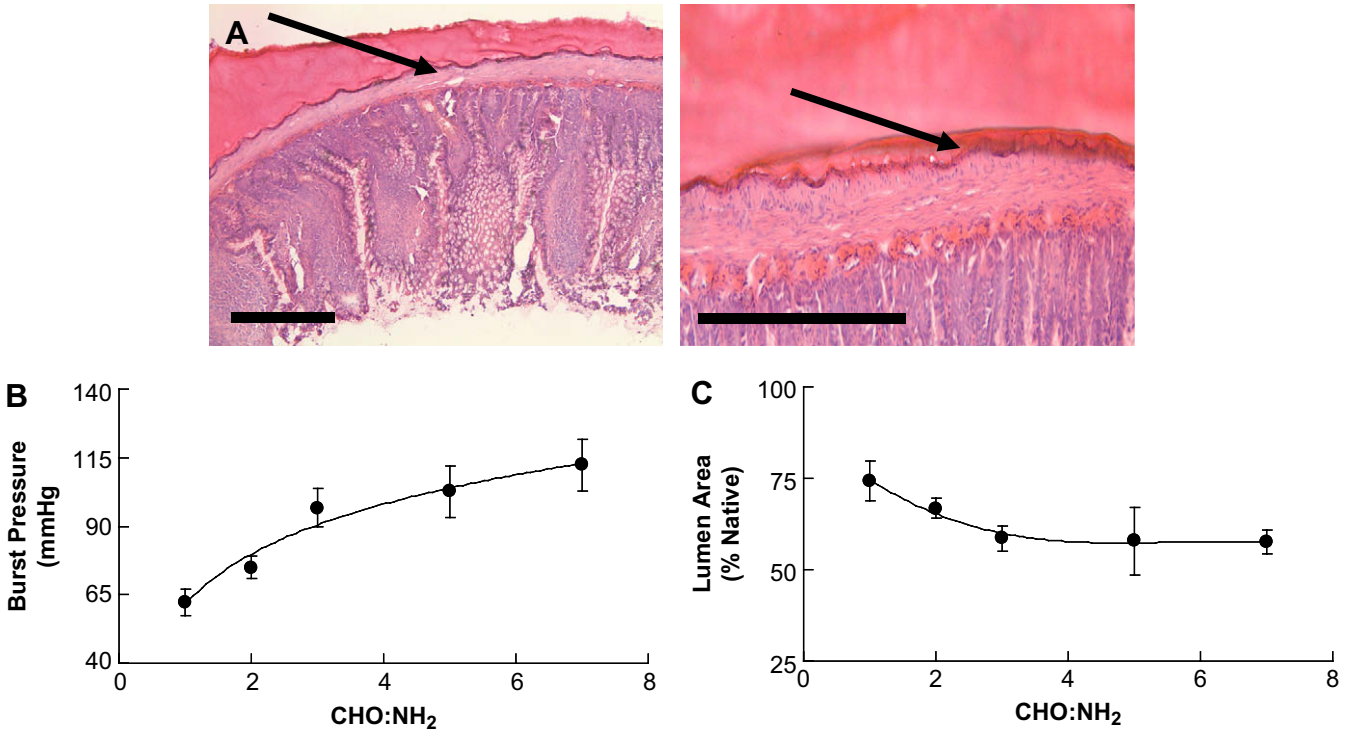

Fig. 1. The tissue–material interface formed between the serosal surface of excised rat duodenum and PEG:dextran appeared continuous after histological processing (cryosectioning, hematoxylin and eosin stain) and microscopic analysis (A, left). Following sinusoidal loading (frequency = 1 Hz, amplitude = 25 mmHg, cycle number = 1000) the interface remained well intact with no indication of material detachment (A, right). Scale bars are 1 mm and arrows indicate the location of tissue–material interface. Burst pressure of wounded intestinal tissue (length = 4 cm) repaired with PEG:dextran nonlinearly rose with CHO:NH_2 across the examined range (B). The percent retention of native lumen area following wound repair and cyclical loading initially decreased with CHO:NH_2 but approached a threshold value (C). Error bars represent 1 standard error of measurement in all graphs ($n = 3$–4).

samples immediately following the mixed injection. The gelation time of each material sample was designated as the elapsed time after injection at which the stir rod rotation was hindered due to the progression of PEG:dextran network formation.

2.8. Stress relaxation of adhesive test elements

The small intestines of adult Sprague-Dawley rats were excised and immersed in buffer as above. Approximately 2 cm-long segments were cut from the duodenum and bisected along the mesenteric line, creating intestinal sheets. Surface samples were constructed by securing an intestinal sheet over a tubular fitting, consistently providing a flat and stable presentation of the outer serosal surface. Samples were inserted into the upper and lower arms of a mechanical testing apparatus configured for tensile testing (Bose® Biodynamic Test Instrument, Minnetonka, MN). A 50 μl volume of test sealant was then applied directly to the lower intestinal surface. The upper and lower intestinal surfaces were immediately brought into contact, and the adhesive material allowed to cure between the tissues for 5 min under a 0.3 N setting force. The tissues and adhesive were subsequently rinsed with 2 ml PBS, with particular focus on the interfacial region. The described tissue–material configuration provided convenient adhesive test elements for analysis under constant tensile displacement.

Stress relaxation of adhesive test elements featuring PEG:dextran, octyl-cyanoacrylate, or fibrin sealant was measured following application of a 0.2 mm step displacement for a 5 min period. Load data were converted to engineering stress and plotted as a function of time, providing a measure of the test element viscoelasticity following tissue–material interaction.

3. Results

3.1. Burst pressure and tissue response following dynamic loading

Excised intestinal tissues were puncture wounded and repaired with PEG:dextran, octyl-cyanoacrylate (CA), or fibrin sealant (FG). Following repair, pulsatile loads were applied to tissue samples through programmed luminal perfusion with PBS. No leakages were detected and all tissue–material interfaces consistently appeared intact and continuous throughout loading. Adhesive failure resistance was quantified through gradual pressurization of sample lumens and reported as the burst pressure of the tissue–material interface. PEG:dextran application burst pressure ranged from 62.2 ± 4.8 to 112.0 ± 9.5 mmHg and rose nonlinearly with CHO:NH_2 (Fig. 1B). The CA–tissue interface had a comparatively higher burst pressure of 132.5 ± 5.8 mmHg, while the FG–tissue interface burst at a lower pressure of 52.0 ± 6.1 mmHg.

Wound repair and cyclical loading consistently induced compressive tissue deformation local to sealant applications. Specifically, the retained intestinal lumen area after PEG:dextran treatment ranged from 57.5 ± 5.74 to $74.2 \pm 9.4\%$ of native dimensions, with increased CHO:NH_2 initially causing more compression but reaching a threshold value (Fig. 1C). CA and FG elicited comparatively more or less deformation, with retained lumen area of $24.2 \pm 0.9\%$ and $84.8 \pm 8.7\%$, respectively.

3.2. Properties of interfacial components in isolation

PEG:dextran materials were studied in isolation to elucidate the dependence of network formation on constituent reactive chemistry. CHO:NH_2 variation imparted order of magnitude ranges of bulk elastic moduli (16.1 ± 0.8 to 161.0 ± 10.8 kPa) and gelation times (6.7 ± 2.5 to 69.2 ± 7.5 s), demonstrating a significant network response to aldehyde density (Fig. 2). Trends in elastic moduli and gelation time illustrate that CHO:NH_2 increase yields stiffer networks which form in less time. However, both bulk properties have a reduced sensitivity to CHO:NH_2 at higher aldehyde content (CHO:$NH_2 > 3$), suggesting that the extent and kinetics of network formation approach saturation at critical concentrations of constituent dextran aldehyde.

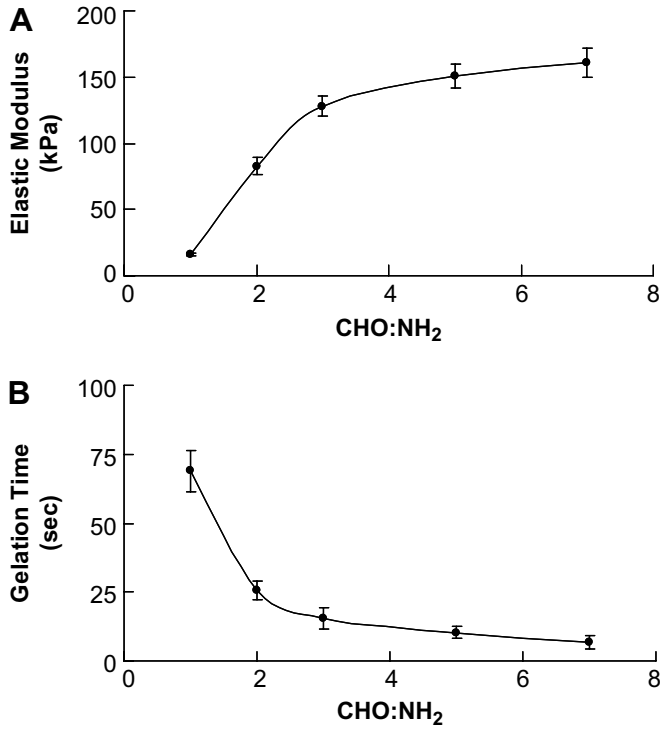

Fig. 2. The elastic moduli (A, uniaxial tensile test parameters of strain rate = 0.005/s, final strain = 0.1) and gelation times (B, 1 ml total material volume) of PEG:dextran are highly responsive to CHO:NH_2, with order of magnitude variances across material formulations. Material properties have reduced sensitivity to aldehyde content when CHO:$NH_2 > 3$, indicating approach to a threshold value. Error bars represent 1 standard error of measurement in all graphs ($n = 3$).

An intermediate PEG:dextran formulation (CHO:NH_2 of 3) and excised intestinal tissue were individually examined under constant strain (Fig. 3). PEG:dextran exhibited notable viscoelasticity, as the instantaneous stress of 28.0 ± 4.3 kPa relaxed to 19.6 ± 2.9 kPa throughout the observation time, while intestinal tissue relaxed more extensively from an instantaneous stress of 20.1 ± 1.3 to 4.9 ± 0.3 kPa. Viscoelastic relaxation mechanisms have presumably evolved in many soft tissues to passively dissipate wall stress under low frequency loading, as particularly characteristic of the digestive process. Both bulk PEG:dextran and tissue relax stress,

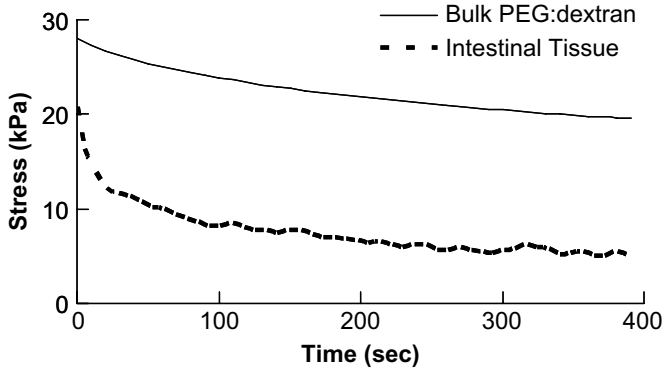

Fig. 3. Bulk PEG:dextran (CHO:NH_2 = 3, sample dimensions of length = 10 mm, width = 8 mm, thickness = 4 mm, $n = 3$) and rat intestine ring samples (ring width = 3 mm, $n = 3$) exhibited stress relaxation in response to a maintained 0.2 strain. The instantaneous tissue stress was approximately 20 kPa, and relaxed to an equilibrium value of 5 kPa over the 400 s observation time. The bulk PEG:dextran was notably stiffer, with an instantaneous stress of approximately 33 kPa partially relaxing to 22 kPa over the same time period.

suggesting that tissue–material adhesive constructs composed of the two may also behave as viscoelastic solids.

3.3. Stress relaxation of adhesive test elements

The viscoelastic behavior of soft tissue adhesion was assessed through the stress relaxation exhibited by tissue–material constructs. Adhesive test elements comprising sealants and intestinal tissue were held at a 0.2 strain, with constant monitoring of resultant loads. All PEG:dextran test elements instantaneously experience a maximal adhesive stress followed by relaxation to an equilibrium value within 300 s (Fig. 4A). PEG:dextran adhesive mechanics were responsive to CHO:NH_2 variation, with instantaneous and equilibrium stress ranges of 2.0 ± 0.2 to 7.1 ± 0.5 kPa and 1.4 ± 0.1 to 3.2 ± 0.5 kPa, respectively. The vertical shift of relaxation curves with increasing CHO:NH_2 parenthetically supports the notion of aldehyde-mediated reactivity with soft tissue. The viscoelastic adhesive mechanics of tissue–material test elements comprising CA and FG bracketed those of PEG:dextran variants, as the former displayed elevated and the latter reduced stresses.

Stress relaxation is derived from the capacity of materials or composite structures to reduce conformational entropy through stress-oriented molecular extensions [27]. Comparison of the instantaneous, equilibrium, and relaxed stress demonstrated that PEG:dextran adhesive constructs relaxed significant fractions of instantaneous stress, with the total amount of relaxed stress generally rising with CHO:NH_2. CA–tissue adhesion achieved high instantaneous stress but underwent minor relative relaxation to reach the equilibrium state, while FG–tissue constructs underwent a substantial relative relaxation but dissipated little overall stress due to a diminished instantaneous response (Table 2).

The stress relaxations of adhesive test elements mimic the response of viscoelastic solids, motivating the use of a standard linear solid (SLS) model to describe adhesive mechanics (Fig. 4B). Model elements consist of a spring (equilibrium arm) arranged in parallel with a spring and dashpot in series (Maxwell arm). Although this SLS modeling approach does not inform on the mechanics of individual interfacial components (two tissue layers, two tissue–material interfaces, and the material layer), it instead lumps together elemental contributions and represents the cumulative mechanical environment following tissue–material interaction. In the following section, stress relaxation data are used to develop, functionalize, and verify a SLS model of PEG:dextran adhesive mechanics.

3.4. Application of the standard linear solid model to adhesive mechanics

3.4.1. SLS model development

The governing SLS differential equation is displayed in Eq. (1), where σ is the adhesive stress and ε is the tensile strain. The model elements and descriptors of SLS mechanics are the equilibrium spring with stiffness K_e [kPa], Maxwell spring with stiffness K_1 [kPa], and Maxwell dashpot with viscosity η [kPa s]. The relaxation time constant τ [s] characterizes the kinetics of viscoelastic adhesive mechanics and is calculated from Maxwell arm components as $\tau = \eta/K_1$. In the following treatment, SLS element descriptors are represented as functions of CHO:NH_2, providing a means of incorporating PEG:dextran compositional information into an adhesive mechanical model.

The constitutive equation is readily solved for the case of a constant strain ε_0, yielding a mathematical description of adhesive stress relaxation (Eq. (2)). Model descriptors are adjusted to fit the experimental data and complete generation of the viscoelastic constitutive equations. The modeled response for each PEG:dextran formulation is plotted along with experimental data as a solid

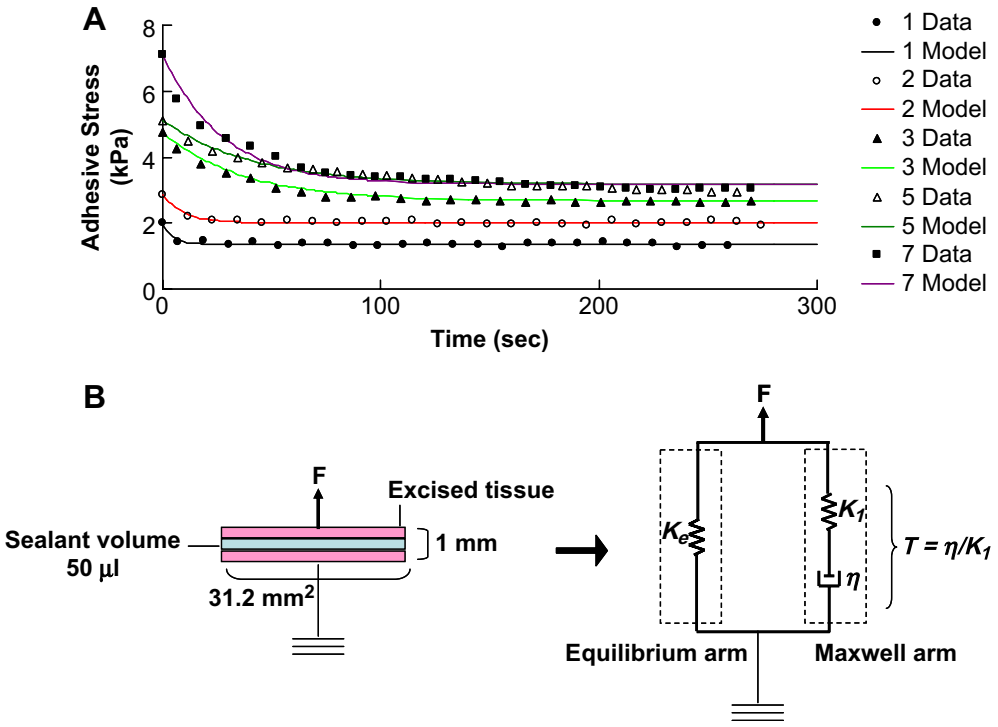

Fig. 4. Stress relaxation of PEG:dextran adhesive test elements (discrete points) closely follow curves (colored lines) generated with mechanical modeling (A, legend numbers denote formulation CHO:NH_2). The viscoelasticity of adhesive test elements (B, left) was modeled with a standard linear solid (B, right). The equilibrium arm features a single spring of stiffness K_e and models time-invariant adhesive mechanics. The Maxwell arm is composed of a spring of stiffness K_1 in series with a dashpot of viscosity η and models dynamic adhesive mechanics.

colored line (Fig. 4A). High Pearson's correlation ($R > 0.98$ in all cases) between the modeled responses and experimental data supports the choice of viscoelastic theory and particularly the SLS to describe adhesive mechanics.

$$\frac{d\sigma}{dt} + \frac{1}{\tau}\sigma = [K_e + K_1]\frac{d\varepsilon}{dt} + \frac{K_e}{\tau}\varepsilon \quad (1)$$

$$\frac{\sigma(t)}{\varepsilon_0} = K_e + K_1 e^{-t/\tau} \quad (2)$$

Equilibrium and Maxwell arm descriptors are plotted as a functions of CHO:NH_2 to delineate the dependencies of steady state and dynamic adhesive mechanics on PEG:dextran composition (Fig. 5). The SLS equilibrium stiffness is interpreted as an indicator of tissue–material reactivity and resultant adhesive bond density, while Maxwell variables reflect the available molecular mobility and stress relaxation following adhesive interaction. The rise of K_e with CHO:NH_2 implies aldehyde-mediated reactivity with tissue, although the nearly identical values of the 5 and 7 formulations (15.8 and 15.9 kPa, respectively) suggest a threshold to the adhesive bond density achievable through isolated variations of dextran aldehyde solid content (Fig. 5A).

Because aldehyde variation was achieved through increase in material solid content, the rise of K_1 with CHO:NH_2 is attributed to the increased number of dextran chains undergoing relaxation both within the PEG:dextran bulk and at the tissue–material interface (Fig. 5B). The inflection of the quadratic τ curve within the examined CHO:NH_2 range demonstrates that adhesive relaxation mechanisms have maximally protracted kinetics at intermediate aldehyde content (Fig. 5C). As τ depends on η and K_1, reduced value at low CHO:NH_2 likely reflects high interfacial and network flow (low η) due to relatively sparse aldehyde bonding with tissue and within the bulk, while low τ at high CHO:NH_2 likely stems from a high aldehyde bond density and extensive molecular relaxation (elevated K_1). Theoretical reasons for these relationships are extended below, along with associated implications for and correlations to sealant efficacy.

3.4.2. SLS model validation

The functional SLS model is validated through correlation analyses of predicted and measured adhesive mechanics featuring PEG:dextran formulations within the examined compositional range (CHO:NH_2 of 1.5, 2.5, and 6). These materials are synthesized with the same polymer constituents described in Table 1, again varying only in solid content of the dextran aldehyde component.

Table 2
Comparison between the instantaneous, equilibrium, and relaxed stress exhibit by adhesive test elements featuring PEG:dextran, octyl-cyanoacrylate (CA), and fibrin (FG) sealants

	PEG:dextran Variants (CHO:NH_2)					Traditional Sealants	
	1	2	3	5	7	FG	OC
Instantaneous Stress (kPa)	2.0 ± 0.2	2.9 ± 0.1	4.7 ± 0.3	5.1 ± 0.4	7.1 ± 0.5	2.2 ± 0.2	11.4 ± 0.6
Equilibrium Stress (kPa)	1.4 ± 0.1	2.0 ± 0.1	2.7 ± 0.3	3.2 ± 0.2	3.2 ± 0.5	1.4 ± 0.3	10.3 ± 0.2
Relaxed Stress (kPa)	0.6 ± 0.2	0.9 ± 0.1	2.0 ± 0.4	1.9 ± 0.4	3.9 ± 0.7	0.8 ± 0.3	1.1 ± 0.5
Relative Relaxation (%)	30 ± 10	31 ± 3.6	43 ± 8.9	37 ± 8.4	55 ± 10	36 ± 14	10 ± 4.3

Entries represent average ± SEM ($n = 3$–5).

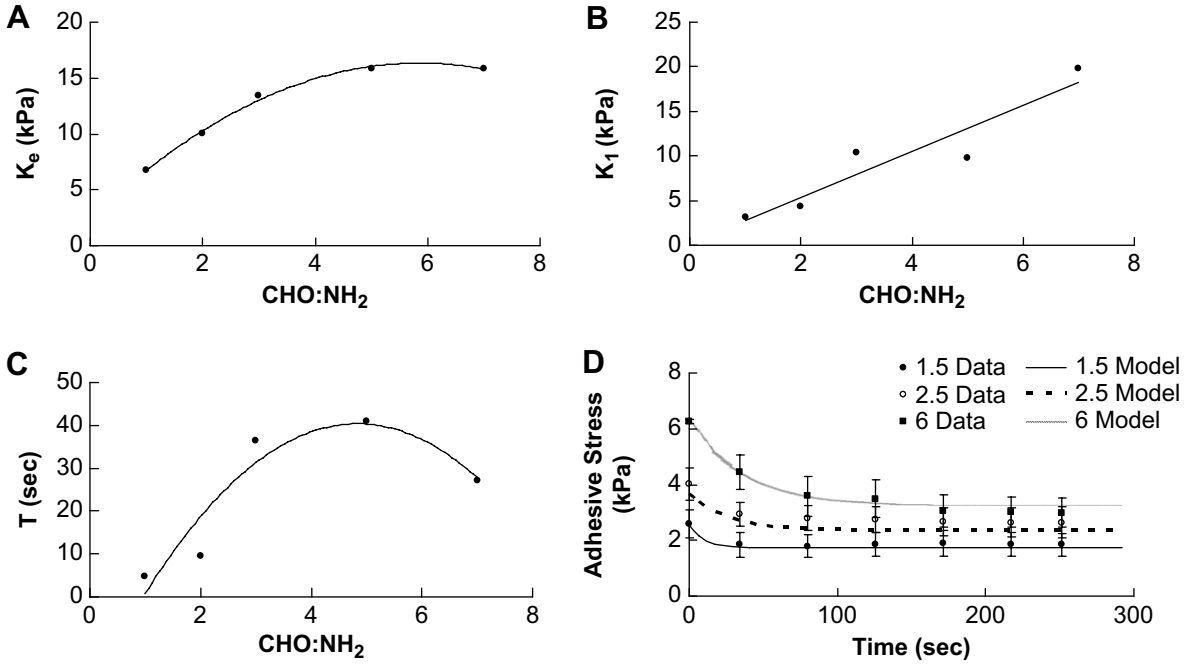

Fig. 5. SLS equilibrium arm stiffness K_e quadratically varied with CHO:NH_2 across PEG:dextran variants ($R = 0.99$), indicating an initial increase and eventual saturation of aldehyde-mediated adhesive bond formation (A). Maxwell arm stiffness K_1 linearly varied with CHO:NH_2 ($R = 0.94$), suggesting that increased aldehyde content enhances the stress relaxation capacity of PEG:dextran adhesive constructs throughout the examined compositional range (B). Maxwell arm time constant τ quadratically varied with CHO:NH_2 ($R = 0.94$), with a clear inflection representing at kinetic maximum within the material design space (C). The viscoelastic responses of PEG:dextran adhesive test elements formed with in-range formulations (CHO:$NH_2 = 1.5$, 2.5, and 6) were predicted based on the above regressions and governing constitutive equations. The modeled responses (lines) correlated well with experimental stress relaxation data (data points) for both PEG:dextran formulations ($R_{1.5} = 0.98$, $R_{2.5} = 0.96$, $R_6 = 0.98$) (D). Error bars represent 1 standard error of measurement ($n = 3$–4).

PEG:dextran formulations with CHO:NH_2 of 1.5, 2.5, and 6 are synthesized with 4.4, 7.4, and 17.7% solid content of dextran aldehyde, respectively.

Predicted adhesive stress relaxation curves for PEG:dextran variants were generated with Eq. (2) and interpolation of model element values. Modeled stress relaxations generated with these methods correlate well to experimental data (Fig. 5D), with a high Pearson's coefficients in all cases ($R_{1.5} = 0.98$, $R_{2.5} = 0.96$, $R_6 = 0.98$). Successful prediction of adhesive mechanics demonstrates SLS parameter continuity within the design space and the potential for strategic adjustment of PEG:dextran composition to meet various application requirements.

3.5. Correlation analyses

Correlations between PEG:dextran material properties and sealant performance metrics suggest a proportional positive influence of increased aldehyde content on both network formation and tissue–material interaction. Specifically, PEG:dextran elastic modulus and gelation time strongly correlated to both wound burst pressure and retained lumen area across the examined range of CHO:NH_2 ($|R| > 0.98$ in all Pearson's correlation two-way analyses). It is important to note that linear correlations generally do not persist if PEG:dextran composition is systematically altered in a fashion other than via aldehyde content. For example, increasing the solid content of constituent PEG amine will dramatically increase the elastic modulus of PEG:dextran without any significant change to adhesive performance (data not shown).

SLS variable descriptor K_e inversely correlated ($R = -0.95$) to the percent retention of lumen area over all PEG:dextran, FG, and CA sealants (Fig. 6A). K_e reflects the equilibrium mechanical state exhibited by a fully relaxed interface and is presumed proportional to the tissue–material adhesive bond density. Inverse correlation to K_e indicates that disturbance of tissue structure is more severe with increased adhesive bonding. Wound burst pressure strongly correlated to K_e with the exception of the CA samples, both reinforcing the import of adhesive bond density and suggesting a role for auxiliary factors (Fig. 6B). SLS modeling facilitated examination of potential secondary mechanical factors, particularly the extent (via K_1) and kinetics (via τ) of available stress relaxation. Linear correlation of burst pressure across all materials is moderately attained ($R = 0.94$) when analyzed against the instantaneous SLS stiffness ($K_e + K_1$) (Fig. 6C). Burst pressure correlation to instantaneous stiffness implicates available adhesive relaxation as an influential factor determining performance, with the capability to entropically dissipate stress improving sealant function. Performance metric correlations to SLS variables suggest that both adhesive bond density and available stress relaxation will together determine overall sealant efficacy.

4. Discussion

Ex-vivo metrics of PEG:dextran sealant performance varied with the constituent aldehyde content and were within the range of clinically available fibrin (FG) and octyl-cyanoacrylate (CA) sealants. Solid modeling of tissue–material test element mechanics effectively described adhesive stress relaxation and distinguished viscous and elastic characteristics governing sealant performance. Correlation analyses of model variable descriptors to performance metrics of PEG:dextran, CA, and FG supported the expected influence of tissue–material reactivity on sealant functionality and tissue response, and also brought forth the benefit of maintaining a stress relaxation capacity after adhesion. PEG:dextran sealants clearly demonstrated aldehyde-mediated adhesion and an substantial capacity to relax adhesive stress in a test element configuration.

Viscoelastic adhesive mechanics imply macromolecular mobility within the tissue, material, and/or interface, and provide

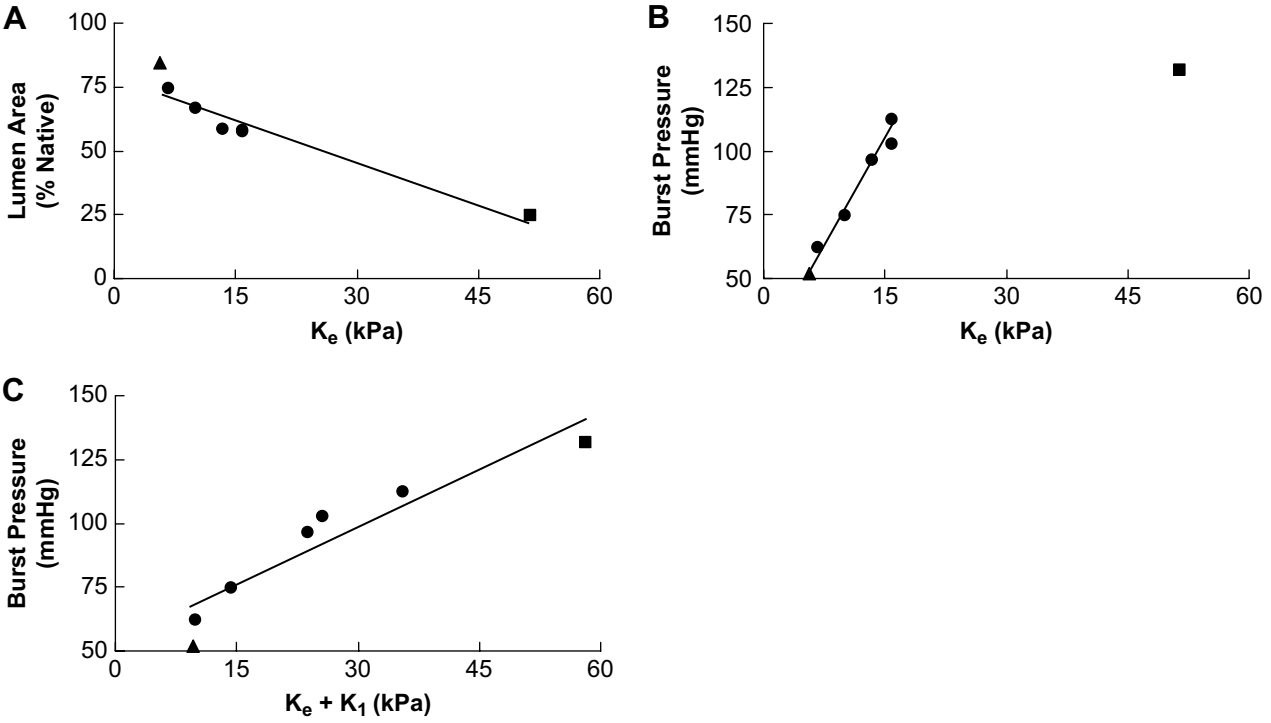

Fig. 6. Performance metric correlations to SLS model descriptors revealed the influence of separable aspects of viscoelastic adhesive mechanics on burst pressure and local tissue response. Equilibrium stiffness K_e inversely correlated ($R = -0.95$) to retained lumen area across PEG:dextran (●), fibrin (FG, ▲), and octyl-cyanoacrylate (OC, ■) samples, indicating that higher adhesive bond density compromised local tissue structure (A). The burst pressure of PEG:dextran and FG repaired wounds had strong linear correlation to K_e, while the CA samples dramatically diverged from this trend (B). Burst pressure across all sealant types showed significant linear correlation ($R = 0.94$) to the instantaneous interfacial stiffness ($K_e + K_1$), implicating the ability to relax stress as an additional factor governing failure resistance following material application and cyclical loading.

a mechanism for entropic dissipation of mechanical work imparted to the application site. If macromolecular mobility is limited by tissue–material crosslinking, adhesive stress will result in an increase of internal bond energies in lieu of an entropic mechanical response. The microscopic breaking of adhesive bonds will occur at a critical bond energy and macroscopically manifest as adhesive failure. Thus, given two equally crosslinked tissue–material interfaces under identical loading conditions, the more viscoelastic interface should have a greater failure resistance by virtue of bond energy minimization. The developed SLS modeling scheme of PEG:dextran adhesion provides a computational tool for predicting viscoelastic mechanics and can facilitate the design of failure-resistant material formulations.

Saturation and eventual loss of all solid-like properties with increasing aldehyde content is expected in the PEG:dextran system. In the limit where CHO:NH_2 approaches infinity, the dextran aldehyde component will remain soluble and formation of a crosslinked gel is lost. Prior to the anticipated compositional threshold, aldehyde-mediated chemistry should play a key role in both PEG:dextran network formation and reaction with tissue and insomuch provide an efficient vehicle for control of bulk and adhesive properties. Strong dependencies of pertinent PEG:dextran properties on aldehyde content clearly emerged throughout this study. Furthermore, property trends indicate that the influences of aldehyde content on the kinetics and end-state of PEG:dextran network formation (indicated via gelation time and bulk stiffness) and adhesive reactivity with tissue (indicated via burst pressure, retained lumen area and SLS equilibrium arm stiffness K_e) are indeed limited and roughly characterized by a sensitivity threshold as CHO:NH_2 exceeds 3.

The plateaus of equilibrium arm stiffness K_e and sealant performance metrics (burst pressure, lumen deformation) with increasing CHO:NH_2 suggests that dextran aldehyde molecules enable gel integrity and tissue seal and are the limiting element in tissue–material interaction. Sealant apposition to tissue can only occur if the aldehyde groups react with both PEG nodes within the gel and tissue sites outside of the gel. The concentration of aldehydes therefore determines the extent of internal gel cohesion and external adhesion to tissue. At a critical CHO:NH_2, increasing dextran aldehyde molecules no longer promotes additional adhesive interactions, possibly owing to steric hindrance of adhesive bond formation. If a clinical application requires more extensive modulation of the above properties, concurrent adjustments of other compositional variables within the PEG:dextran system (for example PEG solid content) will likely be required to compensate for steric effects.

Molecular engineering of PEG:dextran stress relaxation mechanisms could augment aldehyde-mediated adhesion to tissue and improve failure resistance of tissue–material interfaces. Polymer chain mobility and hence stress relaxation could be manipulated through the molecular length of constituent dextran and the grouping of aldehydes along a dextran chain. Longer chains with more distant reactive sites should possess greater molecular mobility and thus entropically dissipate greater amounts of strain energy. Such a material design strategy is distinctly different from simply increasing aldehyde content to improve adhesive strength at the expense of an unfavorable tissue response, an approach which would essentially conform to the established limitations of sealant technologies.

Traditional tissue adhesives and their associated limitations have raised the need for an alternative adhesive system with tunable bioreactivity. Herein we have identified PEG:dextran as a soft tissue adhesive which can be functionally modulated through the constituent aldehyde content. The adhesive mechanical model we utilized relates PEG:dextran chemistry to tissue–material interactions and overall performance. In this specific case the model suggests that viscoelastic adhesion can improve the efficacy of these and other polymeric sealants. In

general such a melding of empiric and modeling approaches may continue to aid in rational application- and tissue-specific material design.

5. Conclusion

The efficacy of soft tissue sealants is limited by sub-optimal extremes of bioreactivity and adhesion strength characteristic of available materials. PEG:dextran hydrogels viscoelastically adhere to tissue to a controllable extent and demonstrate great potential to address current clinical needs. Through systematic analyses of material formulations with graded levels of aldehyde content, we show that PEG:dextran adheres to intestinal tissue largely based on aldehyde-mediated reactivity with the capability to relax stress in the presence of sustained strain. A viscoelastic solid model of adhesive mechanics suitably represents the mechanical properties of tissue–material test elements formed with PEG:dextran and other traditional sealants. Incorporation of PEG:dextran compositional information into the model provides a design tool for strategic adjustment of material composition based on application requirements. Through correlation analyses between pertinent sealant performance metrics and viscoelastic model descriptors, the exploitation of stress relaxation emerges as a potential means of increasing interfacial failure resistance following adhesive applications to soft tissue.

Acknowledgements

The authors acknowledge DuPont, the NIH (GM/HL 49039 to ERE) and the United States Department of Defense for the financial support of this work. Dr. Samuel Arthur provided dextran aldehydes and star PEG amines, Dr. Vijaya B. Kolachalama performed the numerical image analyses, Dr. Aaron B. Baker guided histological analyses, and Dr. David Roylance assisted in the preparation of the manuscript.

References

[1] Buchta C, Hedrich HC, Macher M, Hocker P, Redl H. Biochemical characterization of autologous fibrin sealants produced by CryoSeal and Vivostat in comparison to the homologous fibrin sealant product Tissucol/Tisseel. Biomaterials Nov 2005;26(31):6233–41.
[2] MacGillivray TE. Fibrin sealants and glues. J Card Surg Nov–Dec 2003;18(6):480–5.
[3] Jackson MR. Tissue sealants: current status, future potential. Nat Med Jun 1996;2(6):637–8.
[4] Ellman PI, Brett Reece T, Maxey TS, Tache-Leon C, Taylor JL, Spinosa DJ, et al. Evaluation of an absorbable cyanoacrylate adhesive as a suture line sealant. J Surg Res 2005 May 15;125(2):161–7.
[5] Forseth M, O'Grady K, Toriumi DM. The current status of cyanoacrylate and fibrin tissue adhesives. J Long Term Eff Med Implants 1992;2(4):221–33.
[6] Lamsa T, Jin HT, Sand J, Nordback I. Tissue adhesives and the pancreas: biocompatibility and adhesive properties of 6 preparations. Pancreas 2008 Apr;36(3):261–6.
[7] Singer AJ, Thode Jr HC. A review of the literature on octylcyanoacrylate tissue adhesive. Am J Surg 2004 Feb;187(2):238–48.
[8] Ciapetti G, Stea S, Cenni E, Sudanese A, Marraro D, Toni A, et al. Cytotoxicity testing of cyanoacrylates using direct contact assay on cell cultures. Biomaterials Jan 1994;15(1):63–7.
[9] Kaplan M, Baysal K. In vitro toxicity test of ethyl 2-cyanoacrylate, a tissue adhesive used in cardiovascular surgery, by fibroblast cell culture method. Heart Surg Forum 2005;8(3):E169–72.
[10] Canonico S. The use of human fibrin glue in the surgical operations. Acta Biomed 2003;74(Suppl. 2):21–5.
[11] Siedentop KH, Park JJ, Shah AN, Bhattacharyya TK, O'Grady KM. Safety and efficacy of currently available fibrin tissue adhesives. Am J Otolaryngol Jul–Aug 2001;22(4):230–5.
[12] Silver FH, Wang MC, Pins GD. Preparation and use of fibrin glue in surgery. Biomaterials Aug 1995;16(12):891–903.
[13] Bader RA. Synthesis and viscoelastic characterization of novel hydrogels generated via photopolymerization of 1,2-epoxy-5-hexene modified poly-(vinyl alcohol) for use in tissue replacement. Acta Biomater 4 Mar 2008.
[14] Ciarletta P, Dario P, Micera S. Pseudo-hyperelastic model of tendon hysteresis from adaptive recruitment of collagen type I fibrils. Biomaterials Feb 2008;29(6):764–70.
[15] Fung YC. Biomechanics: mechanical properties of living tissues. 2nd ed. New York: Springer-Verlag; 1993.
[16] Zhang W, Chen HY, Kassab GS. A rate-insensitive linear viscoelastic model for soft tissues. Biomaterials Aug 2007;28(24):3579–86.
[17] Velada JL, Hollingsbee DA, Menzies AR, Cornwell R, Dodd RA. Reproducibility of the mechanical properties of Vivostat system patient-derived fibrin sealant. Biomaterials May 2002;23(10):2249–54.
[18] Alexandre E, Schmitt B, Boudjema K, Merrill EW, Lutz PJ. Hydrogel networks of poly(ethylene oxide) star-molecules supported by expanded polytetrafluoroethylene membranes: characterization, biocompatibility evaluation and glucose diffusion characteristics. Macromol Biosci Jul 2004 14;4(7):639–48.
[19] Groll J, Fiedler J, Engelhard E, Ameringer T, Tugulu S, Klok HA, et al. A novel star PEG-derived surface coating for specific cell adhesion. J Biomed Mater Res A 15 Sep 2005;74(4):607–17.
[20] Sofia SJ, Premnath VV, Merrill EW. Poly(ethylene oxide) grafted to silicon surfaces: grafting density and protein adsorption. Macromolecules 28 Jul 1998;31(15):5059–70.
[21] Irvine DJ, Mayes AM, Satija SK, Barker JG, Sofia-Allgor SJ, Griffith LG. Comparison of tethered star and linear poly(ethylene oxide) for control of biomaterials surface properties. J Biomed Mater Res 5 Jun 1998;40(3):498–509.
[22] Draye JP, Delaey B, Van de Voorde A, Van Den Bulcke A, De Reu B, Schacht E. In vitro and in vivo biocompatibility of dextran dialdehyde cross-linked gelatin hydrogel films. Biomaterials Sep 1998;19(18):1677–87.
[23] Moller S, Weisser J, Bischoff S, Schnabelrauch M. Dextran and hyaluronan methacrylate based hydrogels as matrices for soft tissue reconstruction. Biomol Eng Nov 2007;24(5):496–504.
[24] Bhatia SK, Arthur SD, Chenault HK, Figuly GD, Kodokian GK. Polysaccharide-based tissue adhesives for sealing corneal incisions. Curr Eye Res Dec 2007;32(12):1045–50.
[25] Bhatia SK, Arthur SD, Chenault HK, Kodokian GK. Interactions of polysaccharide-based tissue adhesives with clinically relevant fibroblast and macrophage cell lines. Biotechnol Lett Nov 2007;29(11):1645–9.
[26] Lee JM, Haberer SA, Boughner DR. The bovine pericardial xenograft: I. Effect of fixation in aldehydes without constraint on the tensile viscoelastic properties of bovine pericardium. J Biomed Mater Res May 1989;23(5):457–75.
[27] Ward IM. The mechanical properties of solid polymers. 2nd ed. West Sussex: John Wiley and Sons, Ltd; 2004.